Initial Steps in Modeling of CHEETA Hybrid Propulsion Aircraft Vehicle Power Systems using Modelica

Meaghan Podlaski, Luigi Vanfretti, Abhijit Khare, and Hamed Nademi
Department of Electrical, Computer, and Systems Engineering, Rensselaer Polytechnic Institute, Troy, NY, USA

Phillip Ansell
Department of Aerospace Engineering, University of Illinois Urbana-Champaign, Urbana, IL, USA

Kiruba Haran and Thanatheepan Balachandran
Department of Electrical and Computer Engineering, University of Illinois Urbana-Champaign, Urbana, IL, USA

The aviation industry has been challenged to increase the sustainability of its technologies, which is the main driving force in research and exploration of fully electrified propulsion. This paper presents the initial steps in the design and modeling of the Cryogenic High-Efficiency Electrical Technologies for Aircraft (CHEETA) that would form the basis for hybrid-electric aircraft power systems. To this end, different power system configurations for fully electrified propulsion are proposed and analyzed. Novel, multi-domain components used in both the power system model and the cryogenic thermal system model are introduced and explained in detail. This paper also presents initial results for the different power system configurations under steady-state conditions.

I. Nomenclature

AIM	=	Asynchronous induction machine
A_{cu}	=	Area of copper in the transmission line
BMS	=	Battery management system
CHEETA	=	Cryogenic High-Efficiency Electrical Technologies for Aircraft
EMS	=	Energy Management System
FMI	=	Functional mock-up interface
FMU	=	Functional mock-up unit
G_d	=	Extra heat generation due to faulted HTS line
h	=	Heat transfer coefficient for HTS line
HTS	=	High temperature super-conducting transmission line/cable
I_c	=	Corner current of HTS line
I_c0	=	Corner current of HTS line
MSL	=	Modelica Standard Library
n	=	Intrinsic value of superconducting material in HTS line
PEMFC	=	Proton-exchange membrane fuel cell
PWM	=	Pulse-width modulation
Q	=	Heat loss of the transmission line
SoC	=	State of charge
SOFC	=	Solid oxide fuel cell
T	=	Temperature of LH_2 in the system
T_c	=	Characteristic temperature of the transmission line
TMS	=	Thermal management system
VSD	=	Variable speed drive
$V_{a/b/c}$	=	Three phase voltage
V_{DC}	=	DC voltage
V_{RMS}	=	RMS voltage
ΔT	=	Change in temperature of HTS line

ρ = Resistivity
ω = Frequency of system, measured in radians

II. Introduction

A. Motivation

Future increases in demand for high-speed mobility, sustainability, and profitability requires advancements in aviation technologies. This includes the research and exploration of alternative propulsion and energy sources, including fully electrified propulsion. Simulation-based studies are extremely valuable to determine which concepts and methods are most beneficial. Creating physical prototypes for complex multi-engineering systems can also be costly and difficult; while opportunities for testing using a physical system are limited. As a result, well-defined, reliable models are essential for the development of new aircraft design concepts and/or configurations, prior to their testing. Using state-of-the-art object-oriented equation-based modeling and simulation technologies allows for implementation of models with varying degrees of complexity for individual components or entire sub-systems, which in turn allows system responses to be studied at different levels of detail and for different response times, aiding with early-phase integrated system design optimization.

This research specifically focuses on the application of simulation-based studies for an electrified power system at varying levels of complexity and fidelity, as well as the architecture of a complete multi-domain aircraft vehicle. The models have been created using the object-oriented modeling language, Modelica. Multi-domain models were created to capture each aspect of the power system, including the mechanical, electrical, and thermal domains. This paper introduces the models and libraries used to create the models, modeling flexibility between different levels of model complexity, and preliminary results of the power system models of the fully-electric aircraft concept currently under development by the Center for High-Efficiency Electrical Technologies for Aircraft (CHEETA).

B. Paper Contribution

This paper utilizes the Modelica computer language to develop the multi-domain model of the power system for an electric propulsion aircraft and all of its respective control components. This paper provides initial models, documentation, and initial results for various architectures of a fully electric aircraft. Studies focus on modeling and simulation of a novel electric architecture subject to cryogenic cooling.

C. Related Works

Previous works in this area include the in-depth modeling of the components in aircraft power systems. Previous modeling efforts for hybrid-electric propulsion architectures using Modelica have been successfully applied and studied for the NASA X-57 aircraft [1], which provides a basis for modeling and simulation a new hybrid-electric aircraft using the Modelon Aircraft Dynamics library. The framework for the modeling of electric-hybrid propulsion system architecture in the form of a Modelica library is shown in [2]. Solid oxide fuel cells (SOFC) have been modeled and analyzed using the Modelica language [3], which provided a framework for the higher order fuel cell models in the power system. All of these studies and models provide templates and framework for the development of this aircraft model, allowing us to build off of this work to implement our models. They have been created to have replaceable models used for simulation and analysis, so that the aircraft presented in this paper can utilize these techniques to analyze each subsystem at varying degrees of model fidelity. Model reduction techniques using Modelica [4] have also been utilized, where they focus on simplification of variable transfer and calculation between components in multiple-domain systems and ranking of internal parameter components to speed up calculations. This can be applied to the aircraft to eliminate unnecessary states and reduce the amount of calculations to derive the model response.

D. Paper Organization

This paper is organized as follows. Section 3 outlines the modeling approach using Modelica and need for multi-domain models in this application. Section 4 introduces five different proposed electrical system architectures and their components. Section 5 explains the models used in the proposed architectures in detail. Section 6 presents preliminary results of the five different electrical architectures.

III. Multi-Domain Modeling Approach

Models used in the development of the CHEETA aircraft are created using the object-oriented equation-based modeling language, Modelica. Modelica provides the flexibility to implement and interface models from different engineering domains by developing physically-meaningful equation-based interfaces between them. The term 'domain' refers to an engineering problem, i.e. all electrical variables are connected and modeled according to Ohm's Law, Kirchoff's Laws, and other electrical principles. Mechanical variables are modeled according to laws of mechanical motion, and the thermal variables obey the laws of thermodynamics. Models created using Modelica can also be interchanged by exploiting object-oriented programming principles (e.g. models sharing the same "base class" can be "replaceable" to one another) to analyze models at varying levels of complexity, allowing us to analyze how different modeling assumptions affect response.

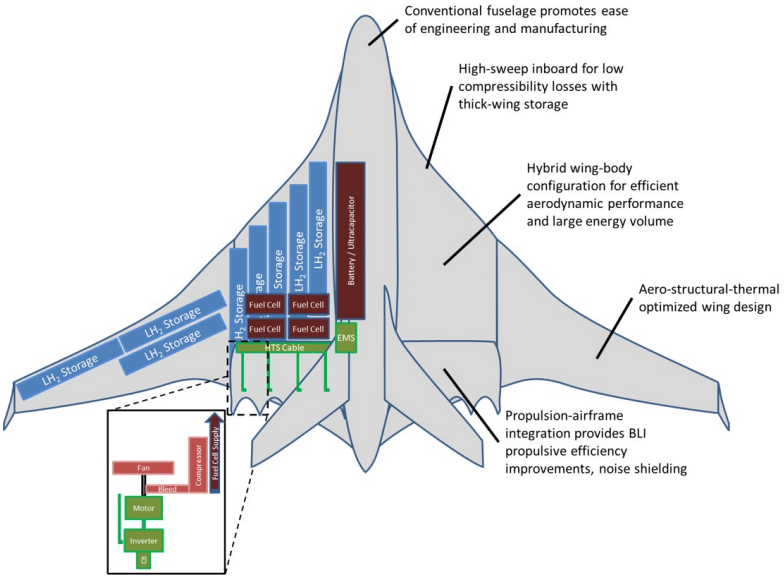

Fig. 1 Layout of CHEETA aircraft in terms of sub-systems and sub-domains.

Given the layout of the aircraft in Figure 1, it is necessary to create interfaces and models to connect each of the sub-systems and components together. In Figure 1, the electrical propulsion system, for example, requires the modeling of mechanical, thermal, and electrical domains. The mechanical domain includes the output of the electric motor and fan, electrical domain includes a high temperature super-conducting (HTS) transmission line, power electronics, and circuit breakers, and the thermal domain addresses models for thermal losses from the HTS line and power electronics and boiloff of LH_2. In this paper, the components in the electrical power system will be modeled and studied.

IV. Proposed Electrical System Architecture Overview

The CHEETA power system consists of a series of fuel cells and batteries supplying DC power to a motor driving the fans for the aircraft. One potential architecture for such power system is outlined in Figure 2. Each group of four fuel cells charges one battery on one bus. The two buses are also connected through a tie line for reliability. Each set of the four motors share one bus connected through a HTS transmission line from the generation bus, which will be cooled using liquid hydrogen. The 1 kV bus bar that connects to all of the fuel cells is cryogenically cooled due to the high currents carried on the HTS transmission lines to the motors.

The battery will be connected at the distribution bus, as shown in Figure 2. This will be done to shift some of the weight off of the fuselage. If the fuel cell bus bar were to fail for any reason, having the batteries directly connected to the motors would provide increased reliability. They would be able to supply temporary propulsion to land the emergency landing gears of the aircraft.

The green boxes above components in Figure 2 represent electrical controls and sensors controlled by the EMS, and the purple boxes represent thermal sensors and controls for the thermal management system (TMS). In this case, all of the fuel cells and batteries will be scaled to also supply power to the additional AC and DC loads shown in Figure 3. The HTS transmission lines that will be cryogenically cooled are designated by the light blue box on top of the line. The orange box on the transmission lines represent a normal transmission line that will not be cooled, since the current is much lower to supply power to the hotel loads and will not produce as much heat.

Additional loads for the aircraft are shown in Figure 3. The main loads considered are for the wing icing protection system, electromechanical actuators, and environmental control system. Additional loads not explicitly considered are lumped into 'other AC loads' and 'other DC loads'. In all other figures of the power system, these loads are reduced to a block labeled 'additional loads' for simplicity.

The cooling for the system is outlined as shown in Figure 4. The motor, HTS lines, and converters will be

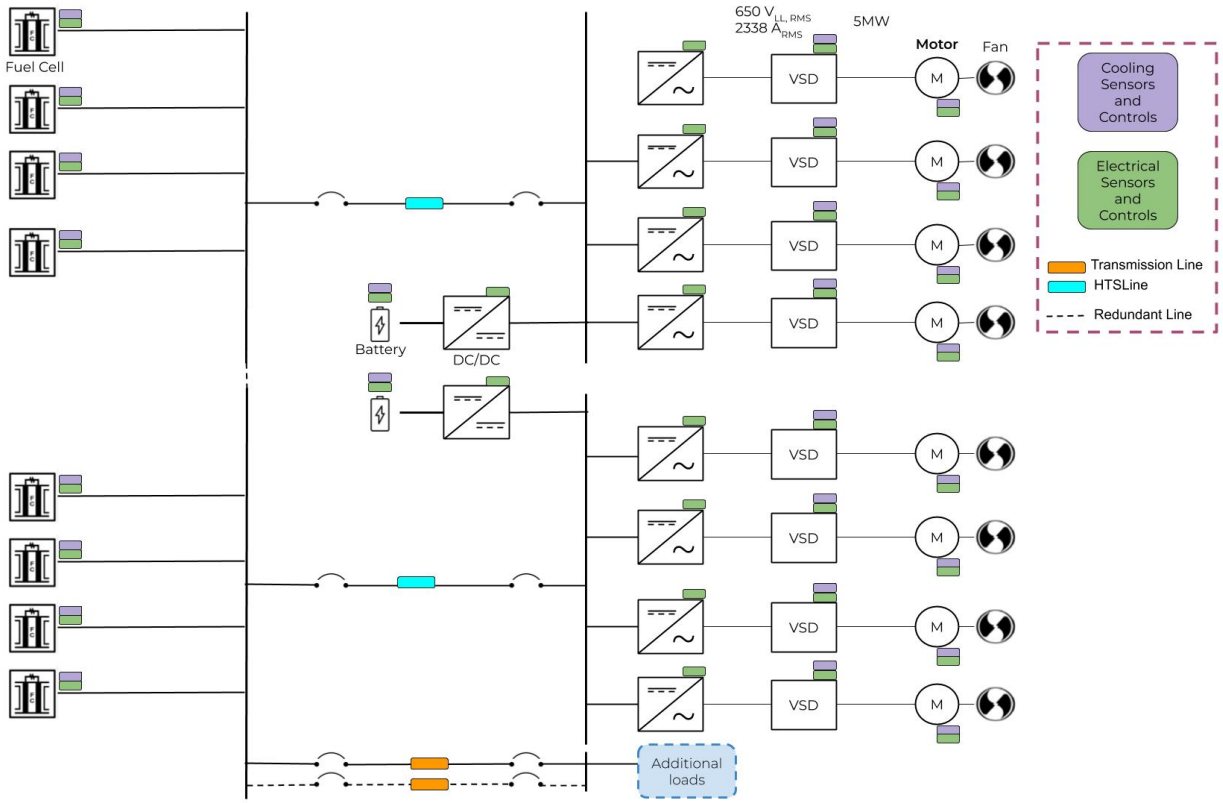

Fig. 2 CHEETA electrical system consisting of eight propulsors with centralized fuel cell power generation. The dashed lines in this case are redundant transmission lines.

cryogenically cooled. There are two loops coming from the LH_2 tank, where the motor is cooled at a temperature of 20K, then the converters are cooled at a temperature of 115K, then the excess cooling goes to the fuel cell. The HTS lines are cooled separately at a temperature of 20-25K. The additional loads of the aircraft in Figure 4 will not be cryogenically cooled.

V. Power System Controls

This paper primarily focuses on the electrical portion of the power system, more detail on the thermal system will be added in the future. The power system controls consist of two parts: the energy management system and the battery management system.

A. Energy Management System

The energy management system (EMS) receives data from each of the components in the power system according to the chart in Figure 5. Sensors will measure the voltage and current at every node in the system, battery state of charge, and flight trajectory in terms of speed to change operating set points. The EMS uses the flight trajectory from either the pilot or cruise control to calculate the reference speed of the VSD. This flight trajectory input will also detect when the aircraft is taxiing, taking-off, and landing so that the BMS can trigger the batteries for discharge. Voltage and current from various points on the system are monitored to maintain safe voltage and current levels for operation and adjust the power flow through the system if there is component failure. The EMS will provide input to the control the pulse width modulation (PWM) for the converters; however, it will not be modeled in the EMS shown here because averaged converters will primarily be used in our simulation studies.

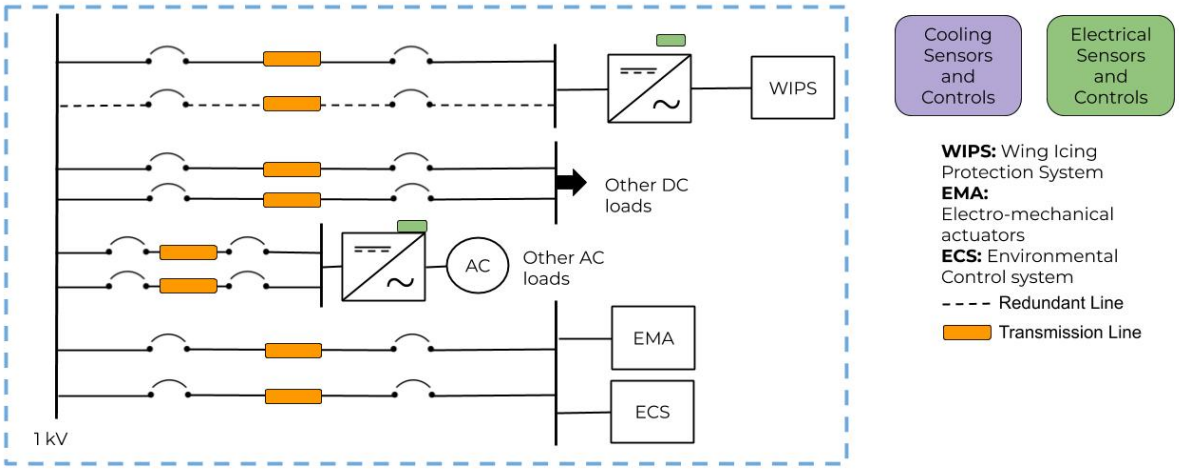

Fig. 3 Non-propulsive electrical loads considered in electrical system.

B. Battery Management System

The battery management system uses components from Dassault System's Battery Library [5]. Figure 6 shows the observer and maximum performance controller that monitors the operation of the battery management system. The observer contains boolean statements to observe the operating voltage, current, temperature, and state of charge (SoC) of the battery. This model provides Boolean outputs that warns the user of under and over voltage, over current, and thermal limits. The maximum and minimum set points for these measurements are defined by the designer or engineer. The battery management system follows the algorithm in Algorithm 1.

Algorithm 1: Battery management system control algorithm.

if $SoC \leq \min SoC$ **then**
  $i_{bat} = i_{charge,max}$;
else if $V_{bus} \leq 0.9 * V_{nom}$ **then**
  $i_{bat} = i_{discharge,max}$;
else if *fuel cell on* == *false* **then**
  $i_{bat} = i_{discharge,max}$;
else
  $i_{bat} = 0$;
end

Figure 7 shows the maximum performance controller. It is a table-based model with values defined in a scientific data format file to define battery charge state, current, and power based off of the maximum and minimum battery state of charge. These tables come from real-world battery systems and are provided in the Battery Library, but will be updated to reflect the CHEETA battery parameters once they are defined.

VI. Power System Models

The electrical power system of the aircraft is modeled in terms of domains as shown in Figure 8, which shows the relationship between the different sub-systems, domains, and the components in the a simplified representation of the CHEETA power system. The blue lines represent electrical connections between components, the red lines represent thermal connections between components, the teal and orange lines are gas and liquid connections specific to the fuel cell, and the gray lines are rotational mechanical connections from the rotor of the machine to drive the fan.

A. Fuel Cell

The fuel cell is developed using the Dassault Systems Hydrogen Library. Both the solid-oxide fuel cell (SOFC) and proton-exchange membrane fuel (PEMFC) will be considered in the power system design. Figure 9 shows the case of the PEMFC operating with the powertrain. There is a block in the bottom of the diagram that expands upon the processes needed to transform the LH_2 to DC power [6], and all of these processes will be modeled using both the Modelon Fuel Cell Library [7] and Dassault Hydrogen Library [8].

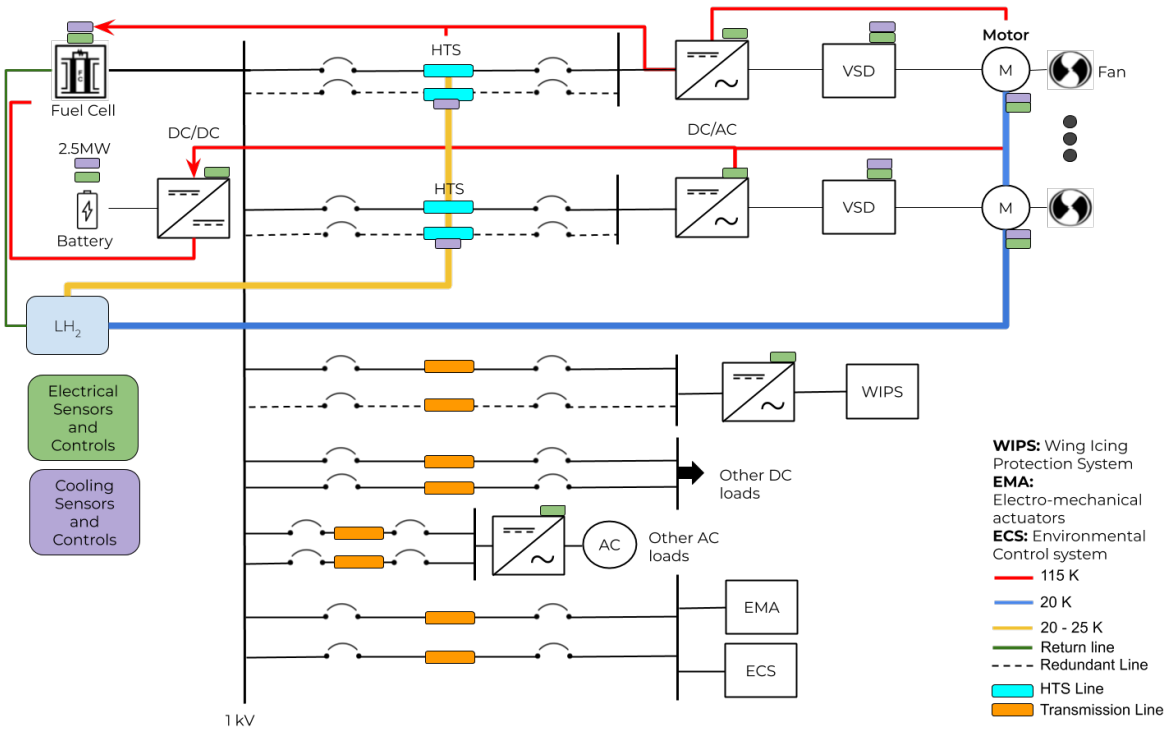

Fig. 4 Initial cooling system concept for the power system.

B. Battery

The battery circuit is shown in Figure 10. The battery charging, discharging, and idle current is controlled by a bidirectional, averaged DCDC converter. The state of the converter is determined by the BMS, which is connected to the converter at input designated as 'i' and receives data through the light blue bus connected to the battery. The cold plates on the battery are held at a constant temperature; in future versions of the model, the thermal system attached to the battery will be included. A more detailed thermal model will be developed in the future.

In Figure 10, the pink external connection is a boolean signal from the EMS to turn on the battery if the fuel cell fails. The dark blue lines are electrical signals with `p1` and `n1` as external connectors to the rest of the system. The BMS uses the voltage and current measurements from the positive external electrical connections to determine the operational state of the battery pack and bidirectional converter. The light blue connection between the `batteryPack` and BMS are used to route the operational measurements from the battery to control the BMS. The red lines are used for the thermal domain to represent the simple cold plate model and interface it with the battery using the `housingHeatPort` component.

The battery for the power system is modeled using the Dassault Systems Battery Library [5]. The library contains models for different cells types. The battery pack currently used in the power system consists of a scaled pack of cylindric cells with constant temperature applied to each side of the housing to represent the cold plates. Figure 11 shows the cylindrical battery pack used in the preliminary power system model. The `cell` block contains the model of the battery cell. It consists of a thermal model, open circuit voltage (OCV) table-based electrical model, and an aging model. The `electricScaling` block is connected to the external electrical connections to the power system and scales the voltage and current through the battery to be calculated per cell. The `housing` and `thermalScaling` blocks that represent the models of the thermal connection to the cold plates. In this paper, we will study only on the electrical behavior of the battery modeling.

C. Electrified Powertrain

The powertrain is modeled using Dassault System's Electrified Powertrains Library (EPTL) [9]. The DC powertrain consists of four parts: an inverter, a modulation method, a motor, and a controller as shown in Figure 8 inside of the expanded block 'C' as components C1, C2, C3, and C4 respectively. The constant parameter block `referenceSpeed` supplies a constant reference speed for the machine that comes from the EMS. A linear speed asynchronous induction machine (AIM) drive is currently being used in the model, but we are also considering using an electrically excited

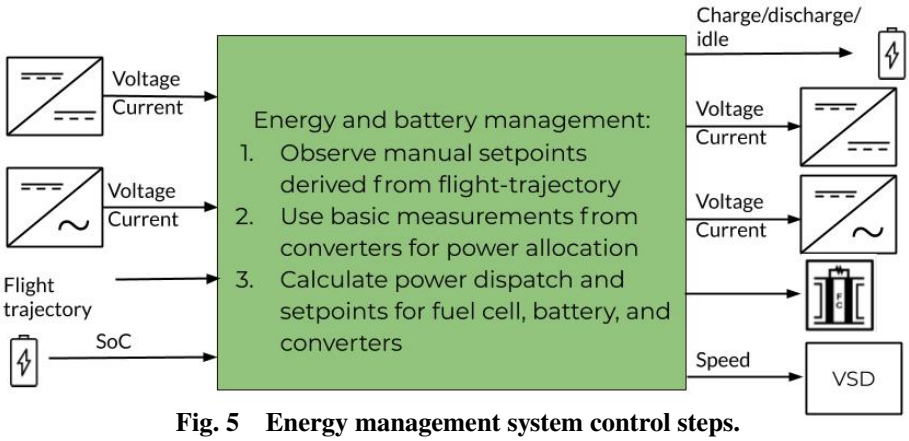

Fig. 5 Energy management system control steps.

synchronous machine drive in the power system since it will be easier to cryogenically cool. In this paper, only models with the AIM drive are shown.

1. Controller

The controller for the electrified powertrain tracks the desired speed of the motor and line voltage to adjust the operating voltage of the machine. Figure 12 shows the PI controller used from the EPTL, which is based off of control Scheme B in [10]. The time constants, limits, and other parameters in the controller are computed from the machine parameters. It contains current controllers, a flux controller, a field weakening controller, a controller for maximum torque, and a block for current limitation.

The `field weakening control` block in Figure 12 sets the reference value for the magnetizing current of the machine based off of the machine's field inductances and nominal flux. The magnetizing current is then used as the input for the `rotor flux estimation` to set the flux producing current. This is calculated by a PI block using the nominal and maximum flux and operating temperature of the machine to determine controller gains. The `current controller` block uses the flux producing current and current from the `speed control` to determine if the machine is operating at maximum voltage. If the machine is not operating at the maximum voltage, the controller will adjust to operating at the nominal flux.

2. Modulation method for inverter control

The `modulationMethod` block (C2) in Figure 8 contains the functions for modulation of the controller signal to supply an input for the inverter. The EPTL has options to use no modulation, sine triangular modulation, and space vector modulation. Currently the model has no modulation method, which is shown in Figure 13. This method just normalized the phase voltages put into the machine with the option to add in a third harmonic distortion.

3. Inverter

The power system is driven by DC power sources, so converters are necessary for maintaining voltage levels and driving the AC machines. Averaged converter models are implemented to eliminate switching functions from the transistors and diodes in the converters to increase simulation speed, however, note that the use of object-oriented features will allow to analyze the impact of both type of converter models within the same architecture. In the future, the inverter model will include parameters for IGBT thermal losses when those details are determined. The calculations for the averaged inverters are shown in Figure 15. The electrical input connections `pin_p` and `pin_n` are connected to the fuel cell/battery input. The signal calculated by Equation 1 is used as an input for `signalVoltage` to produce a three phase voltage. The `signalVoltage` is then connected to external multi-phase connector `plug` to drive the machine.

$$\begin{bmatrix} V_a \\ V_b \\ V_c \end{bmatrix} = \begin{bmatrix} \frac{V_{dc}}{2}\sqrt{2}V_{rms}\sin(\omega t) \\ \frac{V_{dc}}{2}\sqrt{2}V_{rms}\sin(\omega t - \frac{2\pi}{3}) \\ \frac{V_{dc}}{2}\sqrt{2}V_{rms}\sin(\omega t - \frac{4\pi}{3}) \end{bmatrix} \tag{1}$$

The inverter is directly connected to the machine model. Figure 14 shows the model of the asynchronous induction machine modeled as a linear squirrel cage rotor. While the model is not currently configured to include connections of a thermal model, the `AIMC` component interfaces the machine with the thermal system through the red themal poers shown in Figure 14.

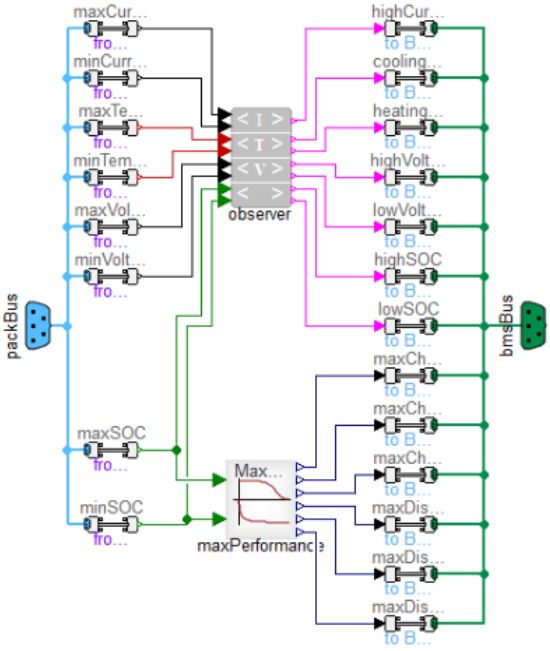

Fig. 6 Battery observer and maximum performance controller as part of battery management system [5].

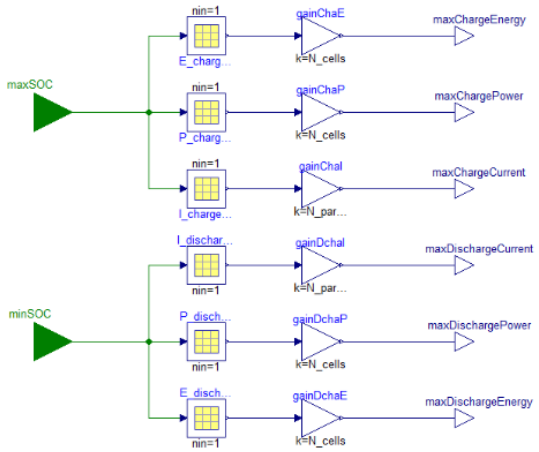

Fig. 7 Maximum performance controller used in battery management system [5].

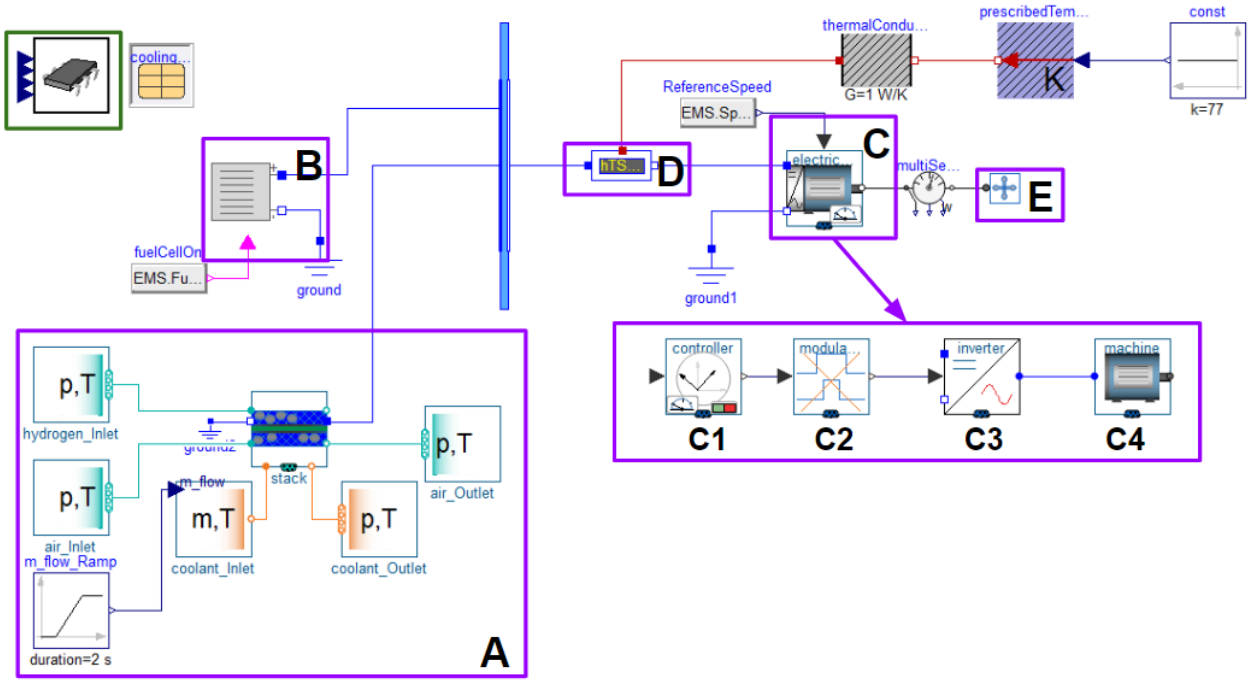

Fig. 8 Single branch of power system modeled using Modelica in Dymola. The letter labels correspond to each subsection of Section VI: Power System Models. The EMS is indicated by the green outline.

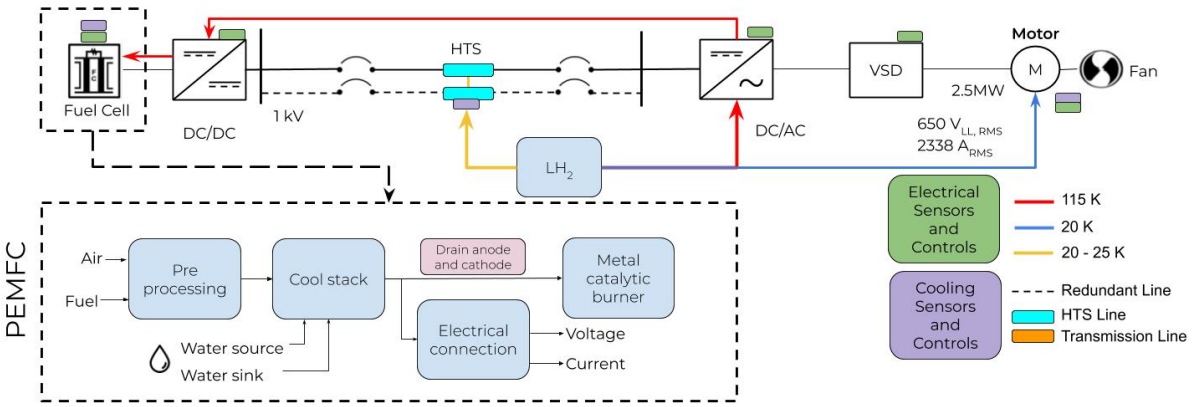

Fig. 9 Power system with fuel cell operating loop. The fuel cell processing subloop is based off of [6].

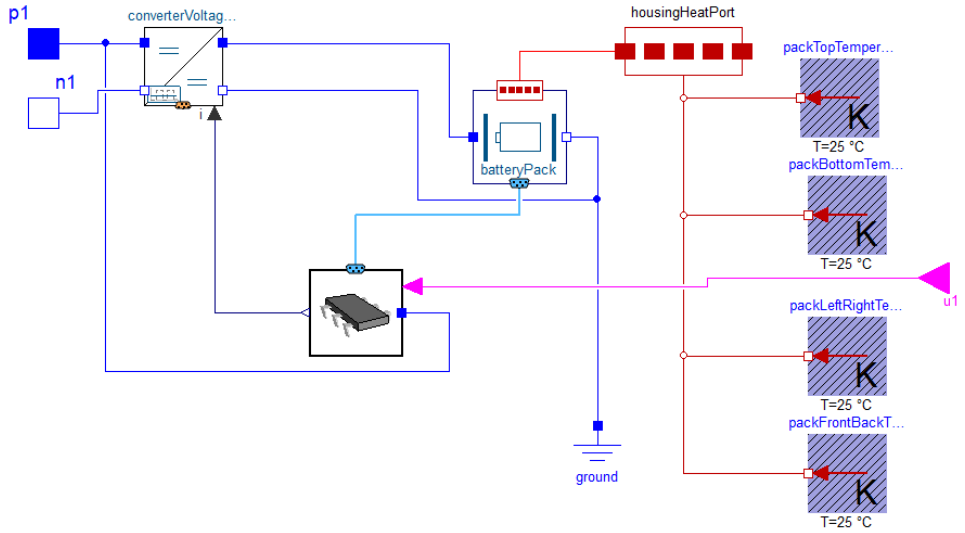

Fig. 10 Circuit for the battery loop in Modelica using Dymola. It consists of the bidirectional DCDC converter, battery, BMS, and simple cold plates to cool the battery.

4. Machine

The blue lines in the model represent the electrical connections in Figure 14 with the AC connection to the inverter from the positive stator plug, labeled as `plug_sp`. The machine model is adapted from the Modelica Standard Library (MSL), which is a library of open-source, standardized models maintained by the Modelica Association[11]. The `spacePhasor` component transforms the AC voltage into phasor form to link to the stator core and inductances. This is then electrically connected to the `airGap` of the machine. The operating temperature and the effect of temperature on the performance will be obtained directly from the coupled 'electro-thermal' analysis.

The gray lines and connections coming out of the `airGap` represent the rotational mechanics of the rotor spinning. This also links to the `friction` component to calculate energy losses due to friction from rotation. The output connector `flange` mechanically links to the fan in terms of torque and rotational angle of the component.

D. HTS Transmission Line and Bus Bars

The HTS transmission line is described using a pi-line transmission line model subject to superconducting behavior using the Stekly cryostability model [12]. The resistance, inductance, and capacitance of the line vary as a function of the critical current carried by the transmission line and the temperature at which the line is kept. The fault behavior and cooling follow the equations outlined in [13]. Equations 2 calculates the corner current for the line as a function of the temperature of the cooling loop. The change in temperature due to the heating of the line is calculated using Equation 3. The heat transfer coefficient `h` is updated continuously during simulation using Equation 4, which can be used to calculate the heat loss of the line in Equation 5.

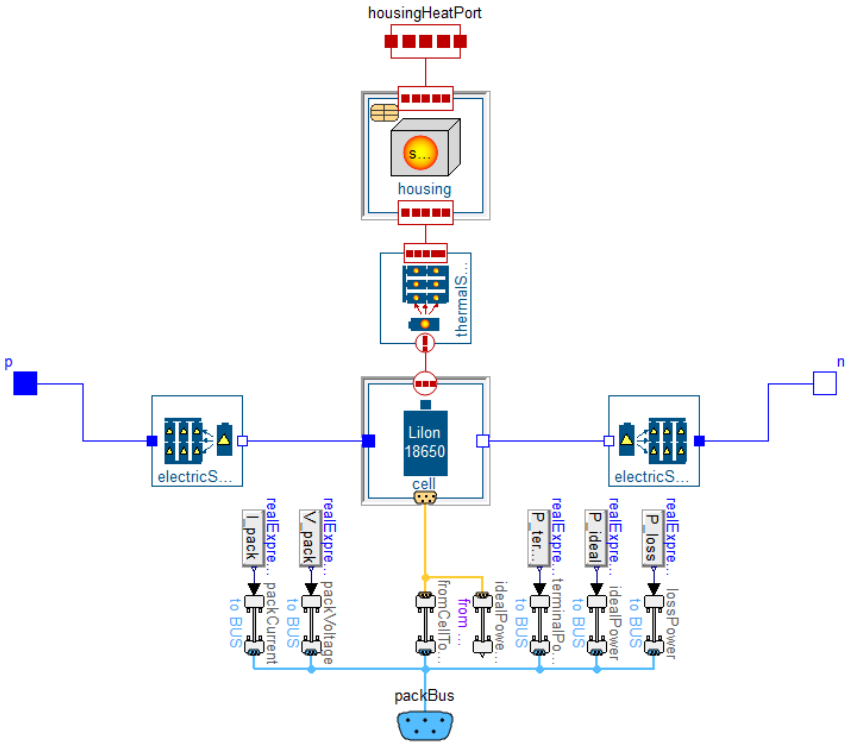

Fig. 11 Cylindric scaled battery pack model from Battery Library [5].

$$I_c = I_{c0}(1 - \frac{T}{T_c}) \tag{2}$$

$$\Delta T = \frac{\frac{\rho I_c^2}{PA_{cu}} + G_d}{h} \tag{3}$$

$$h = 100 * (\Delta T)^n \tag{4}$$

$$Q = h\Delta T \tag{5}$$

The bus bar for the power system will also need to be cryogenically cooled to prevent the conductor from melting from the heat produced by the high currents flowing through the node. The bus bar will also follow similar cryogenic cooling operation using the Stekly cryostability model [12].

E. Fan Load

The motors in the entire power system model drive a fan load, which acts as part of the propulsion system of the aircraft. Currently, only the simplest models for a fan load are available for analysis in the power system model. This model consists of an inertia and a disk to represent the rotational dynamics and weight of the fan. A propeller model similar to the ones available for the drone in [14] and [15] are also included as simple fan models. These propeller models consist of multi-body masses attached to a rotor shaft. In the future, the fan load models will be modeled to fit the fan stalling dynamics shown defined in [16] and [17]. This will allow for the addition of propulsion and other mechanical behaviors to be added to the fan model. The fan model is shown in Figure 16, where the inertia of the fan is converted into a torque that drives a gear that causes two cylinders to rotate. These cylinders are modeled as pipes with a scalar field that changes as a function of time. This assists in the animation and visualization of the fan.

VII. Preliminary Results

The system outlined in Figure 8 is tested using the CHEETA parameters as a single branch. This single branch consists of a fuel cell (operating as a constant voltage source), the HTS line, the powertrain, and a fan. The aircraft is

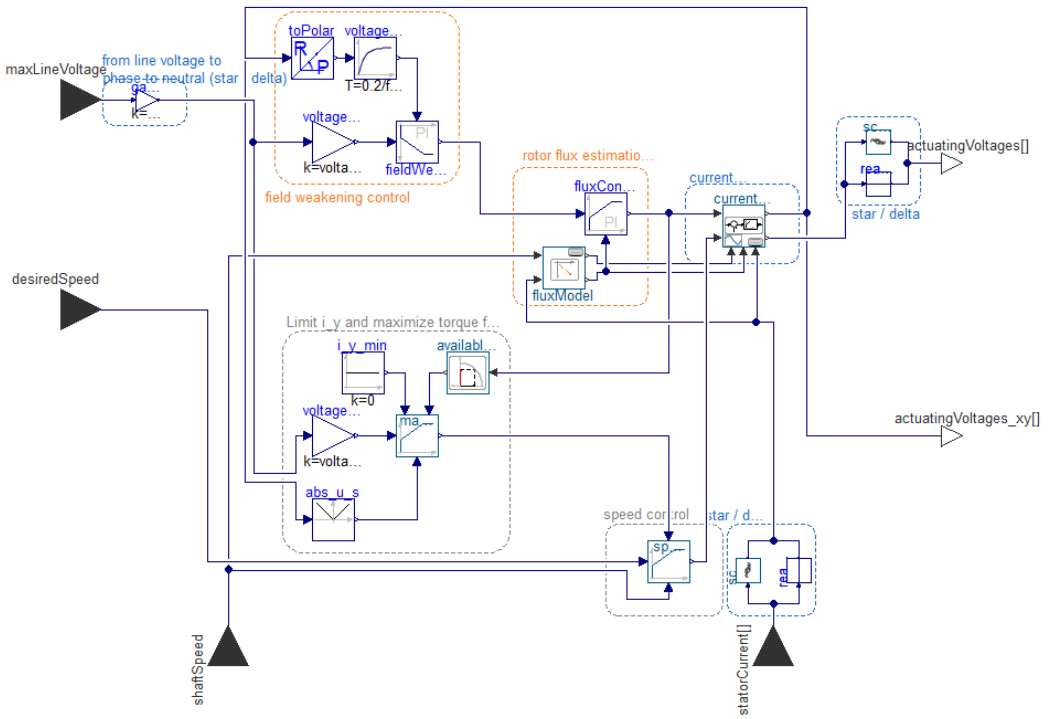

Fig. 12 PI speed controller used in electric speed drive [9].

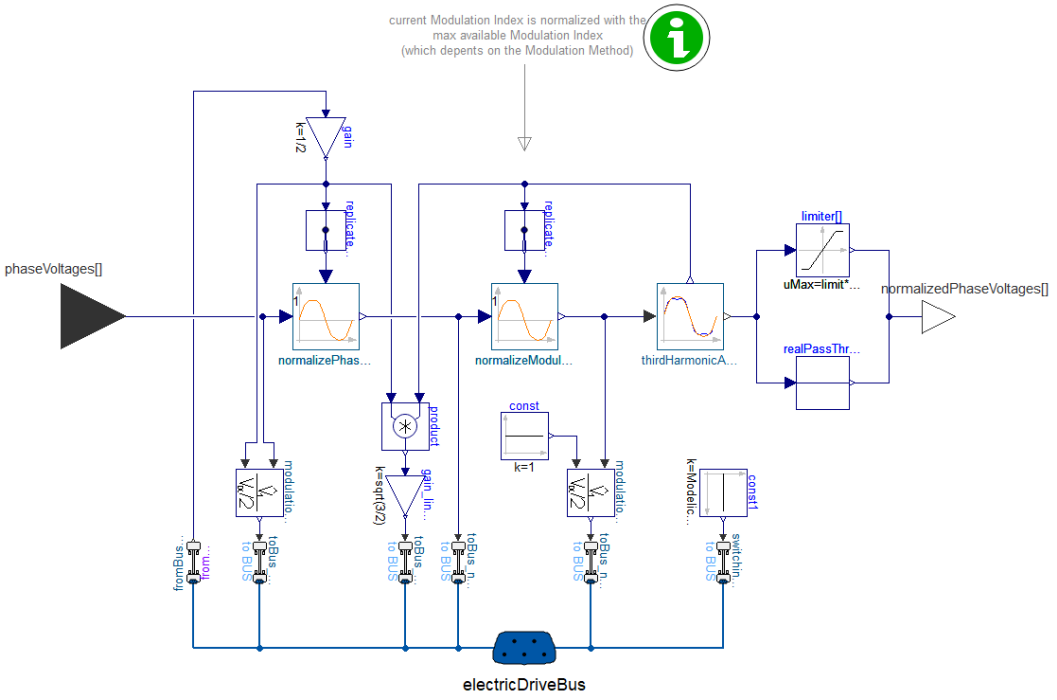

Fig. 13 No modulation method for electric powertrain controller from EPTL [9]. This model takes the phase voltages from the controller and normalizes it to be applied to the inverter.

flown over an hour-long period, where it takes off to a cruising altitude for 2.5 minutes, cruise for 25 minutes, and land for 2.5 minutes. When the aircraft is cruising at a steady altitude, the reference fan speed is 7000 RPM for the 1 MVA machine.

Figure 17 shows the voltage and current applied to the DC side at the drive during the hour long flight. While the AC curves are omitted, the RMS voltage through the machine during the steady state flight is 650 V and the RMS current is

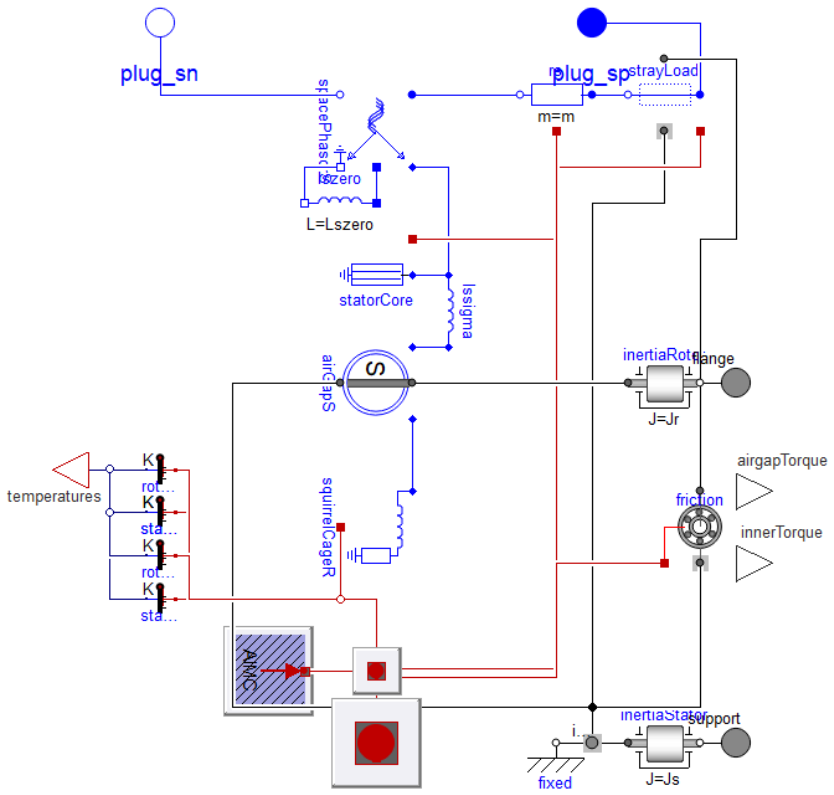

Fig. 14 Asynchronous induction machine from the electrified powertrain [11].

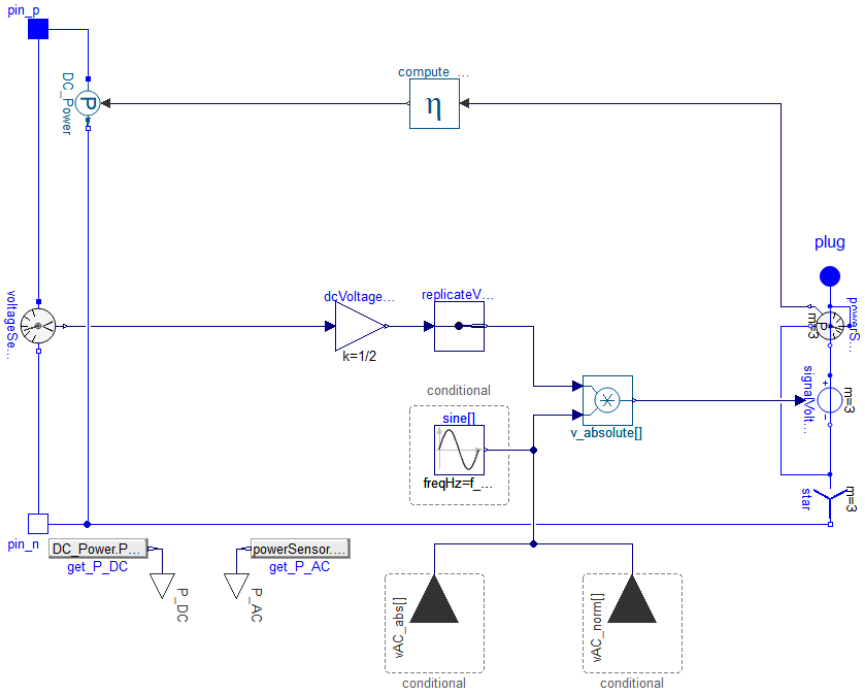

Fig. 15 Averaged inverter from EPTL [9]. The DC voltage from the fuel cell or battery is applied at `pin_p` and `pin_n` and the AC voltage connected to the machine at `plug`. The switching functions from the transistors in a inverter are replaced with the calculations in `dcVoltage`, `replicateVoltage`, and `v_absolute[]` blocks.

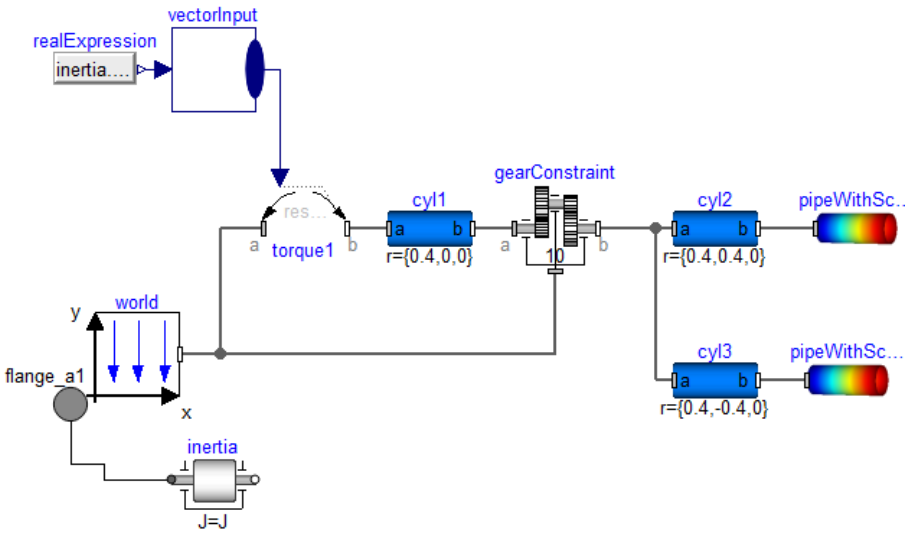

Fig. 16 Modelica fan model. The torque from the motor is applied at `flange_a`, which is applied to the cylindrical blades using the `torque1` component. The `pipeWithScalarField` component visualizes the blades of the fan turning.

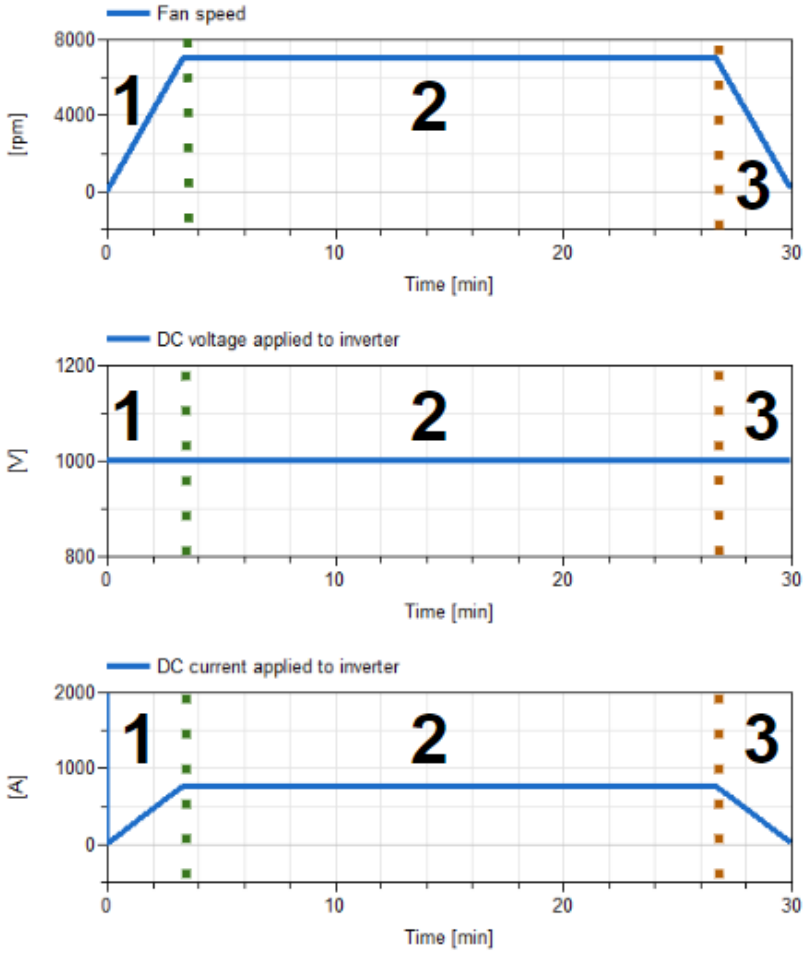

Fig. 17 Machine during half hour flight path. Part 1 is when the aircraft is taking off, part 2 is steady state flight, and part 3 is landing.

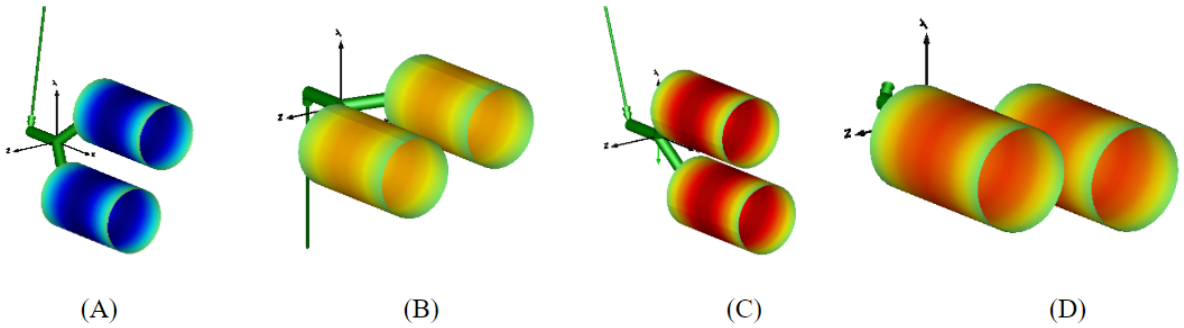

Fig. 18 Fan model animation at (A) 5 seconds (B) 5.6 seconds (C) 5.8 seconds (D) 5.9 seconds with motor moving at a constant speed of 7000 RPM.

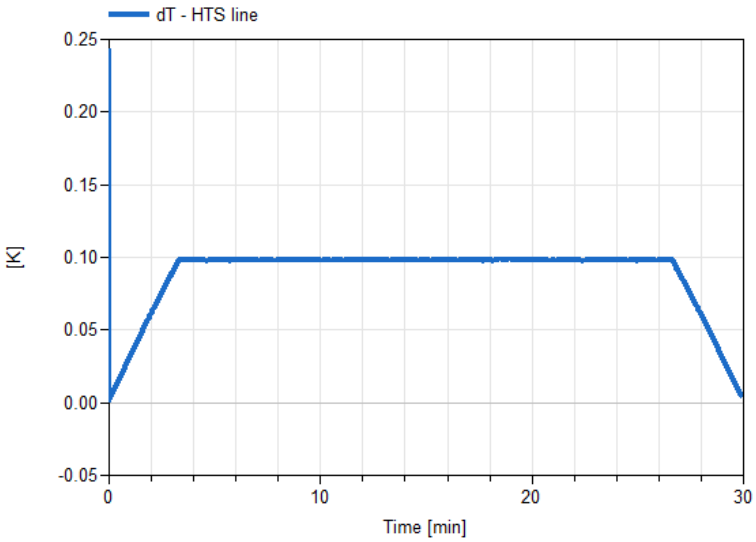

Fig. 19 Change in HTS line temperature during the 30 minute flight path. Any change in temperature less than 2K ensures that the line will operate in the cryogenic region.

850 A. The generator is operating at 1 MVA output. Part 1 is when the aircraft is taking off, it begins to fly at a steady speed during part 2, and is landing during part 3 in Figure 17. In the future, a more accurate machine fan load model will be added to the system to better represent the power draw instead of the approximate inertia model shown in Figure 16.

Figure 19 shows the change in HTS line temperature over the 30 minute flight path. Based off of the mathematical models in [13], the line will be operating safely in the cryogenic region when dT is below 2K. The temperature is maintained by assuming the transmission line is placed in a cooling bath maintained at 20K that can keep the line temperature stable below temperature changes below 2K. The current flowing through the line in Figure 17 is far below the critical current, so the line will not heat up uncontrollably. In the future, the line will be tested to observe the line behavior when faults are applied and the thermal system fails.

The BMS is tested by coupling the battery model in Figure 10 to a fuel cell, which is represented by a cosine voltage source, and a resistive load. This will test the BMS functionality and that the battery will discharge when necessary. Figure 20 shows the cosine voltage source determining when the battery discharges. This verifies functionality of the bi-directional DCDC converter model and the battery. The battery is currently not being dispatched in the overall power system model since the design parameters for the component have not been determined.

The fan model is a multi-domain model that is coupled to the AC motor, designated as blocks ‘E’ in Figure 8. The fan has a multi-body component in it to provide visualization for the fan rotation, which changes the coloring over the time in Figure 18. The green arrow in Figure 18 represents the changing force applied to the rotor of the propeller/fan system.

Using the models outlined and described above, it can be noted that reduced-order models are extremely beneficial for integrated system analysis. If the fuel cell in Figure 8 were replaced with the complete fuel cell models from the

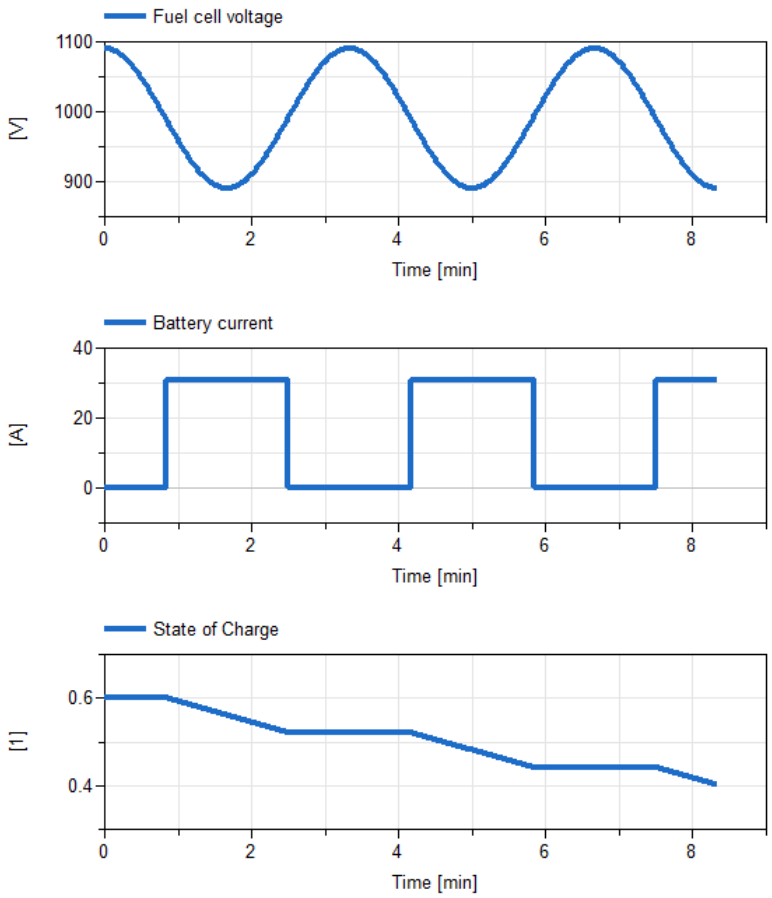

Fig. 20 Battery management system operation. The top graph is the fuel cell voltage modeled as a cosine wave to trigger the battery discharging. The middle graph is the battery current, which discharges whenever the voltage drops below a certain value. The bottom graph is the battery state of charge, which only decreases when the battery needs to turn on.

Fuel Cell Library [3], the integration and simulation time for the system would become prohibitive. The complex fuel cell model has a large number of continuous time states, which causes the integration and initialization of the model to slow down. This same behavior is present in other complex models throughout the power system, showing the need for model reduction and high-accuracy low order models for design.

VIII. Conclusions

This paper provides an outline of the novel components and architecture used in the CHEETA power system with replaceable models of varying degrees of fidelity. The electrified powertain model, for example, can be easily swapped to simulate the power system using different electrical machine models, such as the synchronous and induction motors. The power system has also been tested for a flight path in steady state for proof of concept. In future models, the power system will be tested under fault and component failure conditions to observe reliability of the components and develop more detailed models.

The thermal cooling loop will also be designed and modeled to simulate with the rest of the power system, which will provide useful data on cryogenic cooling of power system components. These cooling models will help give more detail on the thermal losses in the powertrain and generation components. The BMS and EMS will include control based off of thermal inputs.

Acknowledgments

This work was supported in part by NASA under award number 80NSSC19M0125 as part of the Center for High-Efficiency Electrical Technologies for Aircraft (CHEETA), by the Engineering Research Center Program of the

National Science Foundation and the Department of Energy under Award EEC-1041877, by the CURENT Industry Partnership Program, and by the Center of Excellence for NEOM Research at the King Abdullah University of Science and Technology under grant OSR-2019-CoE-NEOM-4178.12.

The first author is supported through a Rensselaer Graduate Fellowship and through the National Science Foundation through a Graduate Research Fellowship.

References

[1] Batteh, J., Gohl, J., Sielemann, M., Sundstrom, P., Torstensson, I., MacRae, N., and Zdunich, P., "Development and Implementation of a Flexible Model Architecture for Hybrid-Electric Aircraft," *Proceedings of the 1st American Modelica Conference*, Modelica Association, Cambridge, Massachusetts, USA, 2019, pp. 37–45. https://doi.org/10.3384/ecp1815437.

[2] Arzberger, M., and Zimmer, D., "A Modelica-based environment for the simulation of hybrid-electric propulsion systems," *Proceedings of the 13th International Modelica Conference*, Modelica Association, Regensburg, Germany, 2019, pp. 471–480. https://doi.org/10.3384/ecp19157471.

[3] Andersson, D., Åberg, E., Eborn, J., Yuan, J., and Sunden, B., "Dynamic Modeling of a Solid Oxide Fuel Cell System in Modelica," *Proceedings 8th Modelica Conference*, Modelica Association, Dresden, Germany, 2011, pp. 593–602. https://doi.org/10.3384/ecp11063593.

[4] Sodja, A., and Zupančič, B., "On using model approximation techniques for better understanding of models implemented in Modelica," *Proceedings 8th Modelica Conference*, Modelica Association, Dresden, Germany, 2011, pp. 697–703. https://doi.org/10.3384/ecp11063697.

[5] Dassault Systems, "CATIA Systems Engineering: Battery Library," , 2020. URL https://www.3ds.com/fileadmin/PRODUCTS/CATIA/DYMOLA/PDF/3DS_2015_CATIA_BTY_Battery__Flyer_A4_WEB.pdf.

[6] James Laraminie, A. D., *Fuel Cell Systems Explained*, chapter and pages, pp. 67–119.

[7] Modelon AB, "Fuel Cell Library," , 2020. URL https://www.modelon.com/library/fuel-cell-library/, [retrieved 15 June 2020].

[8] Dassault Systems, "CATIA Systems Engineering: Hydrogen Library," , 2020. URL https://www.3ds.com/products-services/catia/products/dymola/industry-solutions/, [retrieved 15 June 2020].

[9] Dassault Systems, "CATIA Systems Engineering: Electrified Power Trains Library," , 2020. URL https://www.3ds.com/fileadmin/PRODUCTS/CATIA/DYMOLA/PDF/3DS_2016_CAT_FLYER_EPTL_A4_WEB.pdf, [retrieved 15 June 2020].

[10] Mengoni, M., Zarri, L., Tani, A., Serra, G., and Casadei, D., "A Comparison of Four Robust Control Schemes for Field-Weakening Operation of Induction Motors," *IEEE Transactions on Power Electronics*, Vol. 27, No. 1, 2012, pp. 307–320.

[11] Modelica Association, "Asynchronous induction machine with squirrel cage rotor," Website, 1 2020. Url: https://www.maplesoft.com/documentation_center/ online_manuals/modelica/Modelica_Electrical_Machines_ BasicMachines_AsynchronousInductionMachines.htmlModelica.Electrical.Machines.BasicMachines.AsynchronousInductionMachines.AIM_SquirrelCage.

[12] Z.J.J Stekly and J.L. Zar, "Stable Superconducting Coils," *IEEE Transactions on Nuclear Science*, Vol. 95, 1965, pp. 367–372.

[13] C.J.Kovacs, M.Majoros, M.D.Sumption, and E.W.Collings, "Quench and stability of Roebel cables at 77K and self-field: Minimum quench power, cold end cooling, and cable cooling efficiency," *Cryogenics*, Vol. 95, 2018, pp. 57–63. https://doi.org/https://doi.org/10.1016/j.cryogenics.2018.07.001.

[14] ALSETLab, "Modelica-Drone-3D-FMI," , 2020. URL https://github.com/ALSETLab/Modelica-Drone-3D-FMI, [retrieved 15 June 2020].

[15] M. Podlaski, L. Vanfretti, H. Nademi and H. Chang, "UAV Dynamic System Modeling and Visualization using Modelica and FMI," *The Vertical Flight Society's 76th Annual Forum Technology Display*, Vertical Flight Society, Virginia Beach, VA, 2020 (to be published).

[16] Fink, D. A., Cumpsty, N. A., and Greitzer, E. M., "Surge Dynamics in a Free-Spool Centrifugal Compressor System," *Journal of Turbomachinery*, Vol. 114, No. 2, 1992, pp. 321–332. https://doi.org/10.1115/1.2929146, URL https://doi.org/10.1115/1.2929146.

[17] Moore, F. K., and Greitzer, E. M., "A Theory of Post-Stall Transients in Axial Compression Systems: Part I—Development of Equations," *Journal of Engineering for Gas Turbines and Power*, Vol. 108, No. 1, 1986, pp. 68–76. https://doi.org/10.1115/1.3239887, URL https://doi.org/10.1115/1.3239887.